Astron. Astrophys. 357, 308–324 (2000)

ASTRONOMY AND ASTROPHYSICS

Deep Hα survey of the Milky Way*

V. The l=289° to 295° area

Y.M. Georgelin[1], **D. Russeil**[1,2], **P. Amram**[1], **Y.P. Georgelin**[1], **M. Marcelin**[1], **Q.A. Parker**[2,3], **and A. Viale**[1]

[1] Observatoire de Marseille, 2 Place Le Verrier, 13004 Marseille, France
[2] Anglo-Australian Observatory, Coonabarabran NSW 2357, Australia
[3] Institute for Astronomy, Royal Observatory, Blackford Hill, Edinburgh EH9 3HJ, UK

Received 8 December 1999 / Accepted 11 February 2000

Abstract. An Hα study of the ionized hydrogen in the Galactic plane direction l = 290° has been undertaken. We describe and discuss the characteristics of the numerous filaments and emission patches observed. These appear linked to a major expanding HI bubble or shell over an area of several degrees. Thanks to morphological, kinematical and stellar distance considerations we have linked observed HII regions and molecular clouds into star-forming complexes which mainly trace the Carina arm. We show particularly that the HII regions Gum35 (G289.8-1.3), Gum38b (G291.6-0.5, NGC 3603) and Hf 58 (G291.9-0.7) can be directly linked to the farthest complexes at a distance 'd' of 8 and 9 kpc, while HII regions Gum37 (G290.6+0.3), Gum38a (G291.3-0.7) and the expanding shell can be linked to the closest complexes located between 2.6 and 2.9 kpc. Important internal motions have been identified in the Gum35, Gum37, Gum38a and Gum38b HII regions. The identification and analysis of these motions are essential for a good systemic velocity determination. We have also identified and delineated that part of the Galactic plane exhibiting velocity departures of $\Delta\Theta$ = 7 km s^{-1} (between 285° and 295° and d = 2.5 and 3 kpc).

Key words: ISM: H II regions – Galaxy: kinematics and dynamics – Galaxy: structure

1. Introduction

The Galactic plane area between l = 289° and 292°, located to the east side of the Carina nebula, is very rich in hot stars and HII regions. This zone is well known to contain objects with various distances belonging mainly to the Carina arm (Bok et al. 1970; Georgelin & Georgelin 1970). So far, only the brightest HII regions have been studied in any detail. A complete and coherent study of the ionized gas in this region is still required.

From the main 5 GHz recombination line surveys (with beam size between 4 and 5 arcmin) only the regions with strongest radio flux have been studied (Wilson et al. 1970; Caswell & Haynes 1987), for which CO emission lines and H_2O and OH absorption lines have also been observed. From a whole southern Galactic plane CO survey (8.8 arcmin beam size), Grabelsky et al. (1988) have determined the extent of the identified giant molecular clouds but no details of the molecular structures themselves was obtained.

In addition to the bright HII regions, a large fraction of the ionized hydrogen emission in this Galactic plane area appears as filaments, arcs, patches and diffuse layers. Their wide velocity spread complicates their deconvolution and the study links to the star-forming clouds (molecular clouds - hot stars - HII regions). These links need to be clearly established in order to accurately define the spiral arm structure of our Galaxy. This approach requires both a detailed and more general view of the ionized and molecular gas emission together with kinematic information over the whole area.

Recently, Rizzo & Arnal (1998) have discovered a huge cavity defined by a large, ellipsoidal HI feature expanding at about 22 km s^{-1} centred at l=290.1° and b=0.2°. It is essential to estimate its kinematical contribution by determining if some ionized hydrogen filaments are connected to it. Kinematically, this part of the Galactic plane is well known to exhibit velocity departures from the circular rotation model (several velocities are too negative to be explained by any rotation model). The number of affected objects and the extent of the galactic arms showing these departures are still unknown. It is in this framework that we present a study of this Galactic region which has been observed as part of the Marseille Observatory Hα survey of the southern Galactic plane (MHS) at ESO, La Silla. This survey has produced a large number of 38×38 arcminute images and velocity fields of ionized hydrogen. To extend the study to fine emission structures we have also used high resolution imaging obtained from the AAO/UKST Hα survey (e.g. Parker et al. 1999) which overlaps with our area of study. These two Hα surveys are perfectly complementary (Russeil & Parker 2000).

In Sect. 2, we describe the results of the combined Hα observations and we discuss their implications for grouping the HII regions. We also give, without further interpretation, details of the observed velocities in the large HII regions. Sect. 3 is

Send offprint requests to: Y.M. Georgelin

* Based on observations collected at the European Southern Observatory.

Fig. 1. AAO/UKST Hα survey image of the zone centered at 11^h11^m-60° (coordinates 1950). This image has been obtained from a simple reproduction of the original film HA 18005 (HA 176). The field of view is about 5.5° x 5.5° with north up and east to the left. Lots of unknown filaments, arcs and patches are seen. The high spatial resolution and wide field coverage of the AAO/UKST Hα survey allows us to describe the nature and morphology of several features and to connect large scale structures to smaller ones. For example we can trace large scale filaments all over this Galactic region.

devoted to the extension of the analysis to the radio and stellar data. Results are discussed in Sect. 4.

2. Observations and results

Fig. 1 is a reproduction of the (5.5°×5.5°) Hα film of the AAO/UKST survey field HA176 (exposure HA18005) which covers our region of interest. It uses the worlds largest single-element interference filter (centre 6590 Å, bandpass 70 ÅFWHM). Details of the filter properties and specifications are given by Parker & Bland-Hawthorn (1998). The detector is fine grained, high resolution Tech-Pan film, very sensitive at Hα (e.g. Parker & Malin 1999). This survey, which commenced during 1997, will cover the entire southern Galactic plane from latitudes -10° to +10° with unprecedented arcsecond spatial resolution (Parker et al. 1999). The Hα film studied here shows a spectacular increase of information when compared with ESO Red survey films. Indeed, in addition to the known discrete HII regions, numerous filaments, arcs and patches can be seen over almost the entire field which ocassionally seem to connect HII regions together. Moreover, it appears that the regions named Gum34a,b (G289.1+0.1, G289.6+0.5) (Gum 1955) and Anonymous 4 (G290.8-0.2), 5 (G290.6-0.4), 6 (G290.2+0.2), 7 (290.0-0.7) and 8 (G291.1-1.5) (Georgelin & Georgelin 1970) are in fact some of these filaments.

The MHS on the other hand uses a 36cm telescope equipped with a scanning Fabry-Perot interferometer and a photon counting camera. This instrument is described by le Coarer et al. (1992) and the data reduction method by Georgelin et al. (1994). Each data cube (x,y,λ) obtained has a spatial resolution of 9$\times$9 arcseconds and a field size of 38$\times$38 arcminutes. The most often used Fabry-Perot interference order is 2604 giving a spectral resolution of about 5 km s^{-1}. The Hα profiles observed are always very complex. They are composed of the ensemble of emission lines coming from each emitting layer along the line of sight, each with a potentially different velocity. When the velocity of the emissions is relatively constant over a large area, it is possible to decompose the observed profiles whatever their intensity variation. When, due to significant internal motions, the velocity field of a given HII region is very complex, the profile decomposition is more difficult and can be done only if the intensity of the components is very different. Finally, in the case of very faint and extended regions, the S/N must be increased before profile decomposition. This is done by extracting the profile from a wider area.

Figs. 2 and 3 present the mosaics obtained by the addition of 3 lambda-maps (corresponding to 0.3 Å) of each field centred respectively on velocity V$_{LSR}$=20 km s^{-1} and V$_{LSR}$=-25 km s^{-1}. The difference of these two images is clear and illustrates very well the difference in the distribution of the Hα emissions located at the far (Fig. 2) and near (Fig. 3) distance. In addition to the structured emissions shown in these figures, diffuse emissions are detected even in apparently empty zones of the mosaics.

In order to delineate the spiral structure of our Galaxy we compare our Hα data with that from the radio (see Table 1). Our approach rests on the grouping of HII regions, molecular clouds, exciting stars and OB clusters into large star-forming complexes. This method allows us to minimize, for a given complex, the velocity and distance spread which are caused principally by bulk gas motions and stellar distance uncertainties. Groupings are based mainly on the following points: similar velocity, similar stellar distance and spatial proximity and/or connection by diffuse hydrogen components. The complex systemic velocity separation will be done through identifying the gas motions. The adopted velocity will generally be that of the associated giant molecular cloud. The adopted distance for each complex will, wherever possible, be the stellar one (Sect. 3.2). Indeed, even if very uncertain, the stellar distance depends on no particular gas motions. Details of each complex are summarized in Table 1 and presented Sect. 3.1. The complexes are designated by their galactic coordinates. Since Hα emitting regions are discovered and described by different authors following no set convention it is not possible to use a single identifying nomenclature. We will where possible use the naming convention of Gum (1955) with the IAU designation in parentheses.

2.1. The far complexes

In Fig. 2 the V$_{LSR}$ velocities of the main far regions are indicated. These velocities have been obtained by the decomposition of the observed profiles after identification and subtraction of superimposed components and night-sky lines. For the most prominent regions, Gum35 (G289.8-1.3) and Gum38b (G291.6-0.5) (Gum 1955), which exhibit important turbulent internal motions, only the mean velocity is given in Fig. 2. The detailed velocity field of these regions is presented in Figs. 4 and 5 (the contrast level of these figures has been adjusted to show the detailed morphology of each region).

Using radio data and the information given by the detection/non-detection of diffuse Hα emission with the same velocity between the structured HII regions, it is possible to group the far regions into 3 main star-forming complexes with Gum35, Gum38b and Hf 58 (G291.9-0.7) (Hoffleit 1953) as their respective Hα master regions. Each of these complexes is described below.

2.1.1. The complex 289.3-0.6

Fig. 4 shows the velocity of the condensations and structures constituting the HII region Gum35 (G289.8-1.3). When it was possible to decompose the profiles with 2 components, these velocities are indicated, sorted by decreasing intensity. When greater than 30 km s^{-1} (indicating internal motions), the line width is given between parenthesis. The observed velocity field is very complicated and difficult to interpret. The maximum difference between the velocity of the components is 20 km s^{-1}. From H109α observations, Caswell & Haynes (1987) have obtained a velocity only for the position 289.755-1.152 (10^{h}56^{m}49.4^s, -60°50'32", V$_{LSR}$ = 22 km s^{-1}, ΔV = 29 km s^{-1}). Extracting the Hα profile at the same position into a surface equivalent to their beam size, we find an asymmetric line profile with a barycentric velocity of 11 km s^{-1} and a width of 30 km s^{-1}. This profile can be decomposed into two elementary gaussian lines at 5 and 24 km s^{-1}. In Hα we then detect a blueshifted gas layer while the denser part of the nebula suffers probable extinction by internal dust.

In Fig. 2, between 10^{h}52^m and 11^{h}06^m, a large number of ionized regions (patches and filaments) exist, moreover Gum35, with velocities between 17 and 28 km s^{-1} together with more diffuse emission with the same velocity. Both can be linked to the complex 289.3-0.6. Only 3 of the ionized regions have a known H109α velocity (see Table 1) in good agreement with the Hα velocity. This group of HII regions can be linked to the giant molecular cloud GMC 289.3-0.6 at 22 km s^{-1} (Grabelsky et al. 1988). We note (Table 1) that the CO velocities in the directions of these HII regions are grouped around 2 positive velocities, the first in agreement with the ionized gas velocity, the second one at about 30 km s^{-1}. Wilson et al. (1970) have also found an H109α velocity of 27 km s^{-1} for 289.063-0.355 (10^{h}54^{m}27.9^s, -59°49'39"). This can be interpreted as the probable presence of another molecular cloud 1kpc farther away than GMC 289.3-0.6, as suggested by its velocity.

Table 1. V_{LSR} radial velocities of the star-forming complexes

Name of complex	Name Hα	Name continuum or CO	V_{LSR} Hα (km s^{-1})	V_{LSR} radio rec. (km s^{-1})	V_{LSR} CO (km s^{-1})	V_{LSR} H_2CO, OH, HI (km s^{-1})
288.6+1.5		GMC 288.6+1.5			-22	
289.3-0.6		GMC 289.3-0.6			22	
		289.063-0.355	20	27; 20; 19	28	17/28; 20
	Gum 35	289.755-1.152	14(ΔV=35)	22; 22	11	
	Hf 45-46	289.878-0.792	18	22	19/33;19/33	
		290.487-0.814	20	22	-10/-8/-2/20	
290.1+0.2	Hf 44 (289.5+0.1)		-21		-26/21	
(=Shell)	Gum 34a (289.1+0.1)		-11 to -30			
	Gum 34b (289.6+0.5)		-7 to -30			
	Hα 290.3-0.3		-2			
		GMC 290.2-0.2			-1	
	Hα 290.2-2.0		-7			
	Hα 290.4-1.9		-13			
	Hα 290.5-1.5		-11			
	BBW 336 (290.6-2.0)				-12	
	Hα 290.6-0.5		-33			
	Hα 291.2-0.2		-33			
290.4+1.5	Gum 36 (290.3+1.6)		-20 to -5		-19	
	BBW 343 (290.4+1.0)				-19/-11	
290.4-2.9	BBW 323 (289.8-3.2)				-14	
	RCW 55 (290.3-3.0)		-12		-13	
	BBW 331 (290.4-2.8)				-17	
	BBW 332 (290.4-2.9)				-16	
290.6+0.2	Gum 37	290.646+0.256	-25(ΔV=34)	-28	-24/-18;-35/-18	
290.6-0.2		GMC 290.6-0.2			15	
		SNR 291.0-0.1	(15)			
291.1-1.8		CO 291.1-1.75			-5	
	DC 291.1-1.7					-5
	DC 291.0-3.5				-5	-5
	DC 291.3-1.8				-4	-4
291.3-0.2	An.1 (291.5-0.1)	291.466-0.128	7	6	-7	
	An.2 (291.2-0.1)	291.205-0.267	7	9	-7/ 12	
291.3-0.7	Gum 38a	291.284-0.713	-29(ΔV=35)	-23; -25	-24/28; -21	-26;-22; -26;
	(=NGC3576)					-25/-13/-2
		GMC 293.3-1.4W			-25	
	BBW 348C(292.2-0.2)		-29			
291.4-0.2		GMC 291.4-0.2			-7	
	DC 291.4-0.2					-6.5
291.6-0.7		CO 290.8-0.8			19	
		GMC 291.6-0.4			15	
	Hf 52	291.059-0.770	16	17	15	
	Gum 38b	291.614-0.525	4(ΔV=70)	9; 10;11	-30/13	-27;-28/13;-26/13;-12
	(=NGC3603)					12;-8; -26/-18/-12/-1
		291.910-0.980	14	15	-2/0	
291.7-0.6		CO 290.8-0.8	27		28	
		GMC 291.6-0.5			29	
	Hf 58	291.858-0.675	26	26; 25	30	
292.3-4.9	RCW 58 (292.4-4.9)		-3(V_{exp}=87)			

Table 1. (continued)

Name of complex	Name Hα	Name continuum or CO	V_{LSR} Hα (km s^{-1})	V_{LSR} radio rec. (km s^{-1})	V_{LSR} CO (km s^{-1})	V_{LSR} H_2CO, OH, HII (km s^{-1})
292.4+1.6	BBW 353 (291.9+2.1)				-23	
		MSH 11-54				-19;- 30
	BBW 358A(292.9+1.3)				-22	
292.6-0.3		GMC 292.6-0.3			4	
	Hα 292.0-0.2		4			
293.0-1.0		293.027-1.031		66	-24/ -8/ 57/70	
294.0-0.9		GMC 294.0-0.9			32	
294.0-1.5		GMC 293.3-1.4 E			-25	
	BBW 354 (293.4-0.9)				-24/ -3	
	Gum 39	293.600-1.280	-24	-27	-25	
	Gum 41(294.1-2.3)		-25		-26	
	BBW 361 (294.3-0.1)				-11/-24	
	BBW 363 (294.5-0.4)				-25/-7	
	BBW 365 (294.5-0.3)				-24/-7	
294.1-2.6	BBW 357 (294.1-2.6)				-13	
294.4-0.7		GMC 294.4-0.7			-3	
294.8-1.8	Gum 42 (=IC 2944)	294.837-1.775	-21	-20.9; -18	-18	
		295.06-1.65		-22		
	BBW 362D(293.8-1.7)				-18	
	Gum 40(293.7-1.5)				-18	
	BBW 362G(294.2-1.9)				-19	
295.6+0.0	BBW 372 (295.5+0.5)				-13	
	BBW 373 (295.7-0.3)				-16	

The velocities at 16 and 19 km s^{-1} detected to the north in Fig. 2, around 11^h02^m, can also be linked to the main complex. Indeed, we can see on the CO maps of Grabelsky (1985), velocities around 20 km s^{-1} at longitudes around 289.5° and which are extended to 0.4° in latitude. Also, a faint diffuse emission with similar velocity is detected in the same area.

2.1.2. The complex 291.6-0.7

Gum38b (G291.6-0.5, NGC 3603) is a giant HII region known for its high Hα luminosity and supersonic gaseous motions. It is ionized by a compact cluster rich in O and WR stars. The turbulent motions of Gum38b have been studied by Balick et al. (1980) and Clayton (1986, 1990). With 2 arcmin resolution Balick et al. found supersonic velocities ($\sim$ 40 km s^{-1}) throughout the nebula. They distinguish a highly ionized dense core with line peak velocities blueshifted by 10-20 km s^{-1} with respect to most of the lines from the halo. Clayton, studying the core with high spatial and spectral resolution, found motions of up to 150 km s^{-1} which are not caused exclusively by the action of the stellar wind from the central cluster.

We too find extremely complicated Hα profiles. With our intermediate spatial resolution we cover the entire region which allows us to more easily separate the velocity components of the ionized gas layers located in front of and not linked to NGC 3603. Two such layers are detected with mean velocity -28 km s^{-1} and -12 km s^{-1}, this last one being 2 to 4 times fainter than the first depending on position. These two layers are also detected in absorption (OH and HI) in front of Gum38a and b. The -28 km s^{-1} component, already noted by Balick et al., can be linked to the HII region Gum38a (G291.3-0.6) situated at a distance of 2.7 kpc (see Sect. 2.2). Clayton finds similar velocity components, some of which may be due to this foreground layer, especially in the faint emitting areas to the east of the core.

In Fig. 5, only velocities different from these two foreground emissions have been indicated, i.e. those belonging, with high probability, to Gum38b. Balick et al. found that the lines with positive velocities (i.e. belonging to Gum38b) are spatially restricted to a region of 12 arcmin centred on the exciting cluster. This emission appears more extended, being detected over the whole region of Fig. 5. Similar emission velocities are also detected on a larger scale in Fig. 2. However, it remains difficult to delimit precisely the HII region because it is always very hard to separate the faintest parts of the region from the extended HII envelopes. We detect such a diffuse ionized hydrogen layer with velocity 14 km s^{-1} within 40 arcmin around Gum38b.

Inside the HII region, velocities and intensities are very variable leading to observed line profiles which are very different from one area to an other and thus highly sensitive to the integrated selected surface of the region. However we can note

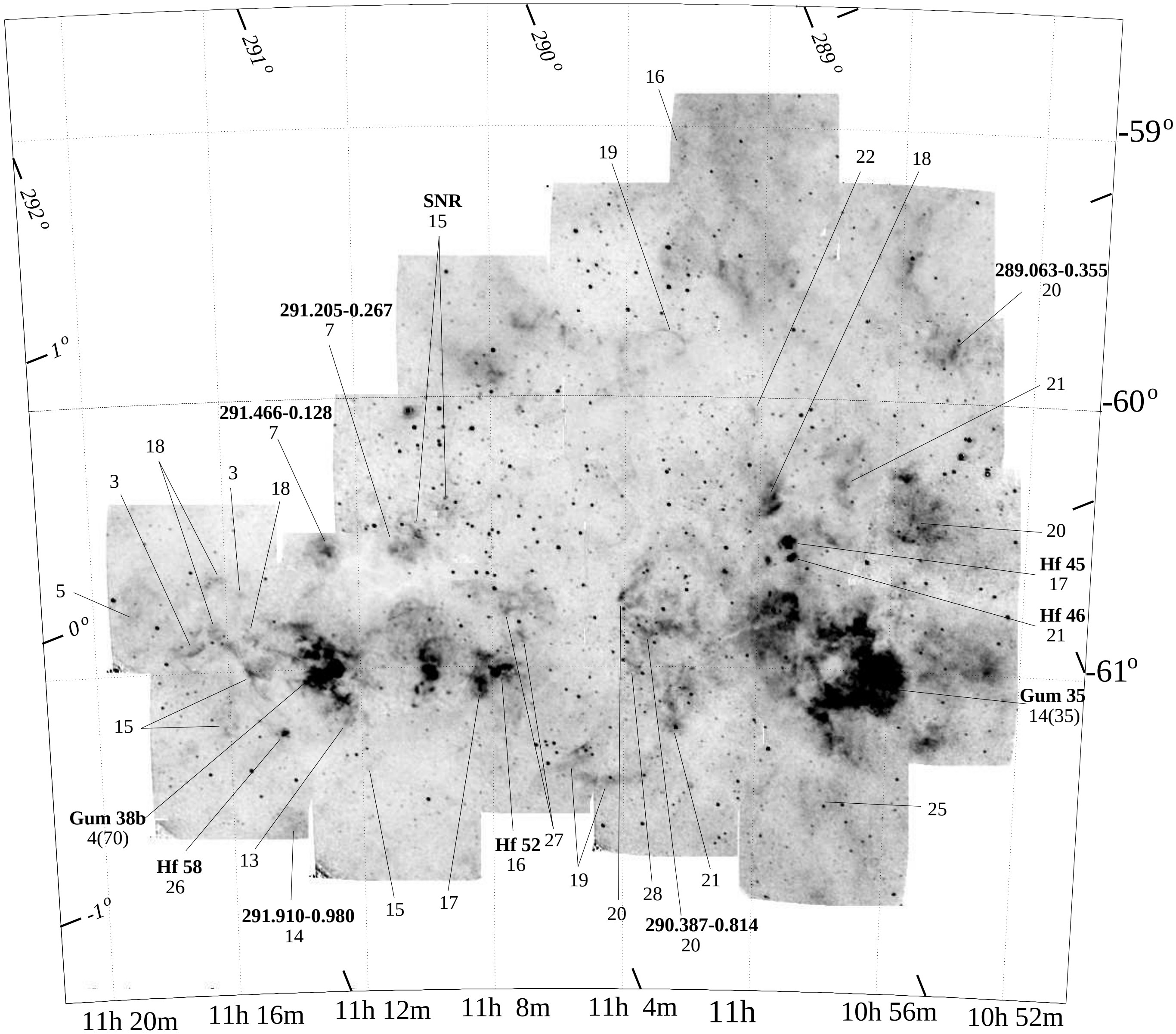

Fig. 2. Hα mosaic of the observed fields at V_{LSR} = 20 km s^{-1}. This image displays the Hα emission located at a distance of about 8 kpc. (Some patches are in fact the residual contribution of HII regions nearer than 8 kpc with important internal velocity motions. It is for example the case of Gum37 (G290.6+0.3) and Gum38a (G291.3-0.7) which appear clearly on Fig. 3.) Each image is obtained adding λ maps (0.3 Å), flat-fielding and then correcting for distortion. The velocities of the Hα emission patches are shown at the point of measurements. Concerning the bright HII regions Gum35 (G289.8-1.3) and Gum38b (G291.6-0.5) the given Hα velocity and line width (indicated between parenthesis) has been measured from the profile integrated all over the entire HII region.

good agreement between velocities extracted at the same position as the ones observed by Balick et al. The lower velocities we observe are around -10 km s^{-1}, but perhaps Gum38b exhibits more negative velocities which are difficult to detect due to the contaminating presence of foreground emissions at -28 km s^{-1} and -11 km s^{-1}. Concerning the higher velocities, they are observed over the entire area and appear the most intense to the north. They reach 50 km s^{-1} and more in the fainter parts located to the north-east of the exciting cluster and brightest regions. This is in agreement with the high velocity components detected by Clayton in his detailed study of the central region. Balick et al. concluded that the core and the halo were kinematically distinct. However, from the velocities we have obtained, the kinematics seem more complicated. The Hα velocity given in Table 1 and in Fig. 2 has been obtained by integrating the core and the halo. The adopted systemic velocity is 13 km s^{-1} from the molecular velocities. This velocity is in agreement with those found in the external regions of Gum38b.

The giant molecular cloud associated with Gum38b is GMC 291.6-0.4 with velocity 15 km s^{-1} (Grabelsky et al. 1988). The HII regions 291.910-0.980 ($11^h13^m51.4^s$, -61°31'11") to the

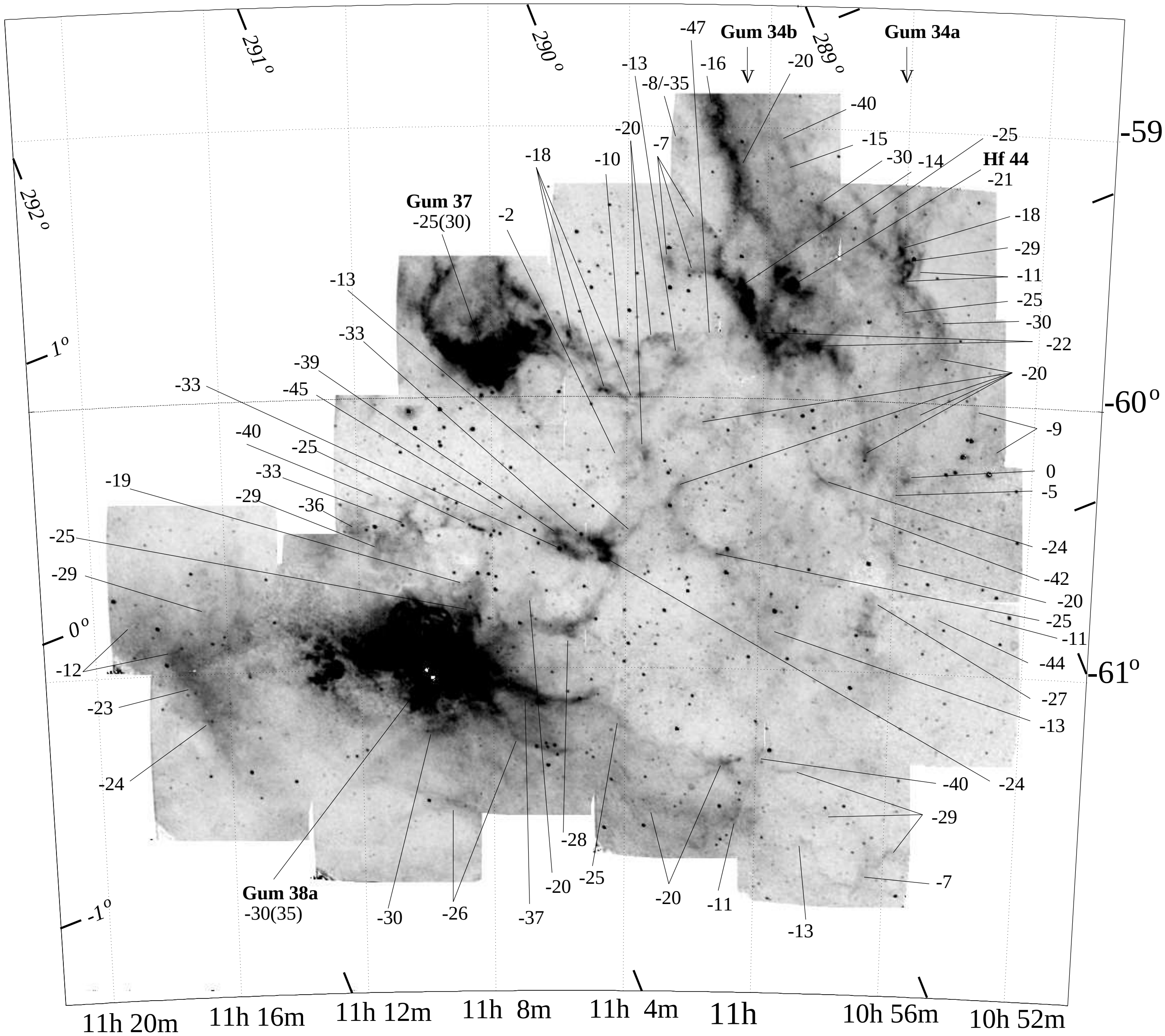

Fig. 3. Hα mosaic of the observed fields at V_{LSR} = -25 km s^{-1}. This image displays the Hα emission located at a distance of about 2.7 kpc. We can see that, in addition to well defined HII regions, a large part of the Hα emission exhibits filamentary structures. These structures are part of a large Shell already known in HI. Each image is obtained adding λ maps (0.3 A), flat-fielding and then correcting for distortion. The velocities of the Hα emission patches are shown at the point of measurements. Concerning the bright HII regions Gum37 (G290.6+0.3) and Gum38a (G291.3-0.7) the given Hα velocity and line width (indicated between parenthesis) has been measured from the profile integrated over the entire HII region.

south and Hf 52 (G291.1-0.8) and the neighbour bright regions located to the west of Gum38a also belong to this complex.

2.1.3. The complex 290.6-0.2

In the direction of GMC 290.6-0.2, with V= 15 km s^{-1}, no similar Hα and H109α velocities have been detected. Grabelsky et al. (1988) suggest that this cloud is probably the superposition of two clouds at 9 and 18 km s^{-1}. The SNR 291.0-0.1 (Roger et al. 1986), corresponding to Anonymous 3 in Georgelin & Georgelin (1970), is located at the border of this giant molecular cloud. This SNR is superimposed on filaments linked to the HI bubble (see Sect. 4) at 60°30'. Due to the velocity spread of these filaments, it is difficult to determine those belonging to this SNR. Nevertheless, the regions corresponding to 843 MHz radio continuum maxima, exhibit additional Hα velocity components around 15 km s^{-1} ($11^h09^m10^s$-60°18', V_{LSR}=15 km s^{-1}, $11^h10^m20^s$-60°24', V_{LSR}=18 km s^{-1}, $11^h11^m10^s$-60°32', V_{LSR}=14 km s^{-1}, and the central part $11^h09^m50^s$-60°32', V_{LSR}=16 km s^{-1}).

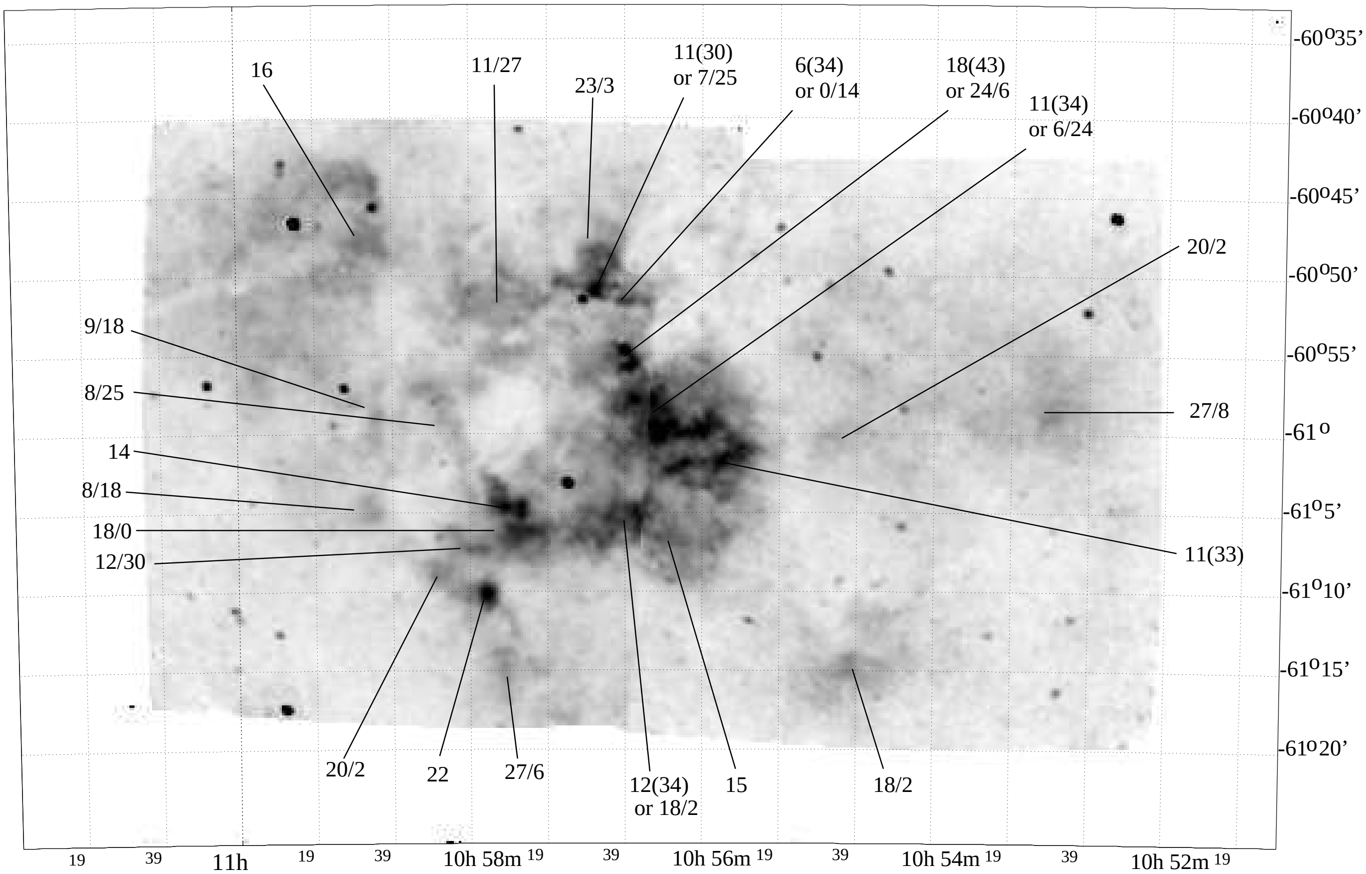

Fig. 4. Monochromatic image of the giant HII region Gum35 (G289.8-1.3). The velocity of the main condensations and zones have been indicated and correspond either to the barycentric velocity of the line or, when it was possible to decompose profiles into 2 elementary components, to the 2 velocities sorted by decreasing intensity. In addition, when greater than 30 km s^{-1} (indicating strong internal motions), the line width is given between parenthesis.

2.1.4. The complex 291.7-0.6

Hf 58 (G291.9-0.7) is a small HII region linked to GMC 291.6-0.5 with CO velocity 29 km s^{-1}, located farther than the previous complex. Between $11^h06^m20^s$ and $11^h09^m00^s$ and -60°40' and -60°48' we find an ionized cloud with velocity 27 km s^{-1}. Close-by (290.8-0.8) in the CO maps of Grabelsky (1985) two molecular clouds at 19 km s^{-1} (this one is a part of the 291.6-0.7 complex) and 28 km s^{-1} are evident. This last CO cloud is probably linked to the ionized hydrogen at 27 km s^{-1}. We thus link this ensemble to the 291.7-0.6 complex because of its similar velocity rather than to the 289.3-0.6 complex.

2.1.5. The other positive velocities

The H109α regions (291.466-0.188 and 291.205-0.267), corresponding to the Hα regions Anonymous 1 and 2 (Georgelin & Georgelin 1970), have a velocity of 7 km s^{-1}. In Hα Anonymous 2 has an additional component at -29 km s^{-1} which is a part of the near complex (see Sect. 2.2). In fact, the Hα regions in this zone are very complicated morphologically and kinematically. The close proximity of the SNR 291.1-0.1 complicates the kinematics by superimposing its components. The CO velocities of Russeil & Castets (2000) show no CO emission at 7 km s^{-1} but show components at -7 km s^{-1} (which can be linked to the near dark cloud 291.4-0.2) and 12 km s^{-1} (which is probably linked to the complex 291.6-0.7). Moreover, Anonymous 2 seems to be excited by the cluster NGC 3590 though the layer this cluster is exciting (that at +7 km s^{-1} or -29 km s^{-1}) is not identified. For these regions we can't currently choose between the following possibilities: they formed an independent group at the kinematic distance of 7 kpc, they belong to the shell discussed in Sect. 4 or they are linked to Gum38b.

Finally, the Hα velocities at 3 and 5 km s^{-1} found towards 292.0-0.2 may be due to ionized hydrogen emission linked to the molecular cloud n°19 of Grabelsky et al. (1988) (GMC 292.6-0.3) at V=4 km s^{-1}.

2.2. The near complexes

In Fig. 3 we have indicated the negative velocities. The velocity spread is significant and it is impossible to deduce a coherent picture. Indeed, close patches on the sky sometimes exhibit drastically different velocities whatever the position on the mosaic. Many regions, especially among the brightest ones, have velocities between -20 and -30 km s^{-1}. The highest velocities are

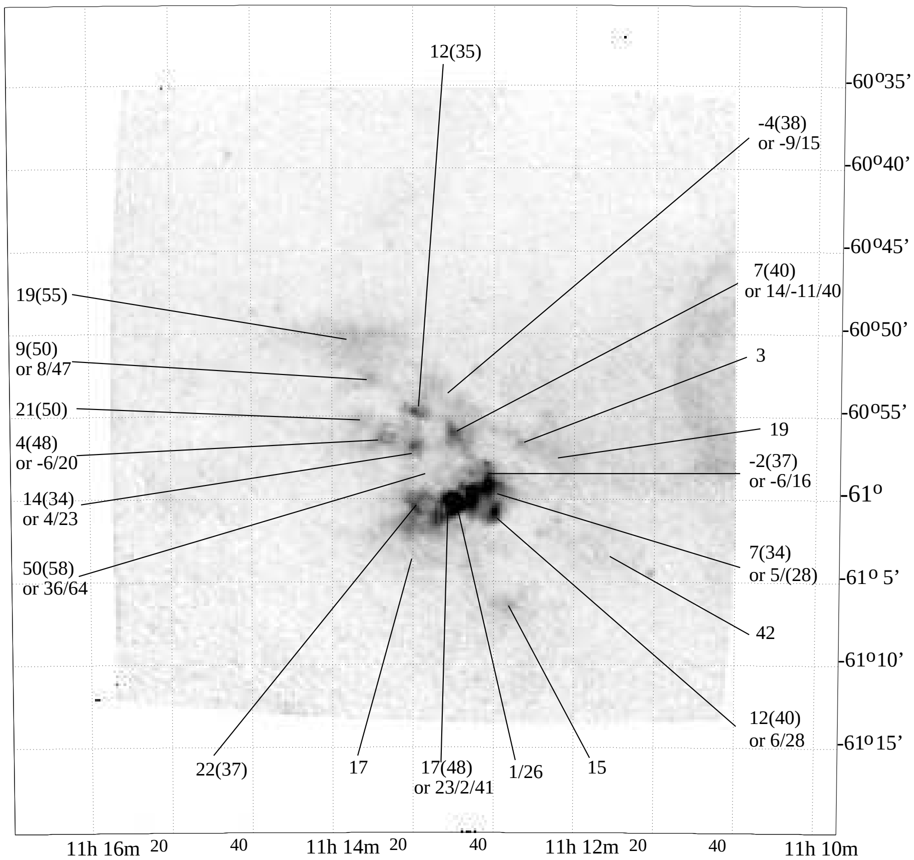

Fig. 5. Same as Fig. 4 for the HII region Gum38b (G291.6-0.5, NGC 3603). The foreground components at -28 km s^{-1} and -11 km s^{-1}, present all over the region, have been omitted.

around 0 km s^{-1} while the most negative ones reach -47 km s^{-1}. We now discuss the most prominent regions.

2.2.1. Gum34a,b (G289.1+0.1, G289.6+0.5)

From Fig. 1 it is clear that these regions, assumed to have their own exciting source, are in fact composed of the accumulation of bright filaments. This is corroborated by the observed Hα velocities: velocities are homogeneous within filaments or sections of filaments but different from one filament to another, varying between -10 km s^{-1} and -40 km s^{-1}.

2.2.2. Gum37 (G290.6+0.3)

Fig. 6 displays the monochromatic emission (bandwidth 15 km s^{-1}) centred at -25 km s^{-1} of Gum37 and the different Hα velocities observed inside it. In this figure we have indicated (by decreasing intensity) two elementary components with FWHM of 25 km s^{-1} fitted to the profile when it was sufficiently assymetric, else the profile barycentric velocity and width are indicated. The uniform layer at -5 km s^{-1}, detected all over the field, has not been indicated. This HII region clearly exhibits an expansion. The maximum velocity separation of the two components reaches 25 km s^{-1}. The maximal line widths are found at the south towards the cluster NGC 3572. The main stars of this cluster, which are probably the sources of ionization of Gum37, are not located in the more intense part of the HII region but a little to the south. Only the star HD 97222 (B0.5II) is located in a bright part of Gum37. The hottest star of NGC 3572, HD 97166, is a O7.5IIIf star and the ionized hydrogen surrounding it exhibits two gas layers with a velocity difference of 20 to 25 km s^{-1}. This suggests that the expansion motions of Gum37 are probably due to stellar winds from the cluster stars. The small ring like nebula at $11^h08^m27^s$, -59°58'44", found by Phelps & Janes (1991), has a velocity of -25 km s^{-1}. This confirms that this HII region and the nearby peculiar shaped nebulosities are related to Gum37 in agreement with the results of Noumaru & Ogura (1993).

2.2.3. Gum38a (G291.3-0.7)

Gum38a (often named NGC 3576) is an optically intense HII region with unusual morphology: a core composed of several knots (NGC 3581 and NGC 3582) and a system of arcs and filaments located to the north. In Fig. 7 the velocities obtained from the different parts of this region are indicated. As suggested by its morphology, the kinematical analysis shows significant internal motions. Most of the observed profiles can be decomposed with 2 elementary components. Inside the filamentary part the two components have a velocity of about -10 km s^{-1} and -36 km s^{-1}. The maximum velocity difference reaches 45 km s^{-1} to the north of the core where filaments seem to originate. The possible known exciting stars are listed in Table 2. As suggested by Girardi et al. (1997), the listed stars located in the core are not

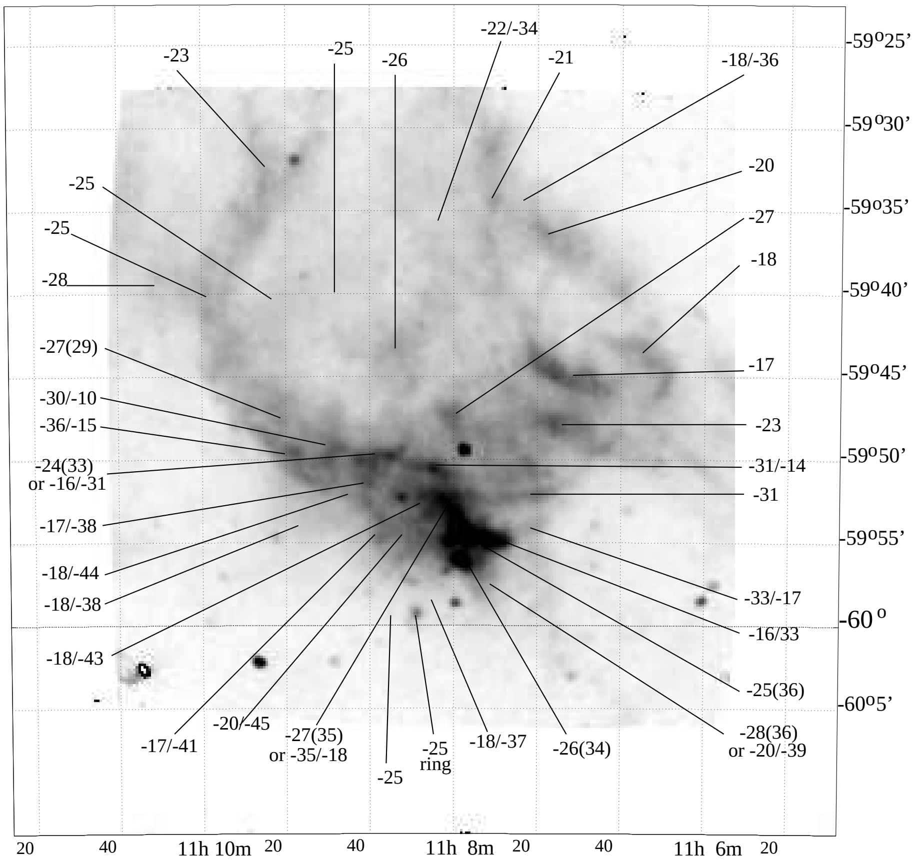

Fig. 6. Same as Fig. 4 for the HII region Gum37 (G290.6+0.3). The component at -5 km s^{-1}, present all over the field, has not been indicated.

hot enough to be the main sources of excitation. From near-IR photometry, Persi et al. (1994) deduced the presence of a very young massive star cluster deeply embedded in the molecular cloud. They suggest that the star formation started further out of the molecular cloud and has progressed to deeper parts. In such a model the motions we observed can then be explained by the stellar winds from the first star generation.

2.2.4. The diffuse hydrogen

In addition to the structured HII regions, seen in Fig. 3, the ubiquitous diffuse emissions appear as widely extended components with uniform velocity. One of these diffuse emissions exhibits a velocity range between -20 and -30 km s^{-1}. It can be linked to the bright regions Gum38a and Gum37. The other component has a velocity between 1 and -12 km s^{-1}. The -12 km s^{-1} velocities are found between 11^h04^m and 11^h14^m and -60° and -61° close to Gum38a. Note that emission patches with similar velocity are also present elsewhere in the mosaic as illustrated in Fig. 3.

3. Velocity and distances of the star-forming regions

3.1. Velocities

Table 1 gives the velocities of different objects (HII regions and/or molecular clouds) gathered together into star forming complexes between longitude 289° and 295°. Note that among the complexes described, some are giant star-forming regions while others are only single small HII regions. The table's contents are described below.

Column 1: Name of the star-forming complex grouping the objects listed in Column 2.

Column 2: Identification of the optical HII regions: Gum (Gum 1955), Hf (Hoffleit 1953), RCW (Rodgers et al. 1960), BBW (Brand et al. 1986 or Brand 1986), DC dark clouds (Hartley et al. 1986) and Hα followed by the galactic coordinates for features identifiable in Figs. 2 and 3. To aid in the identification of these regions their names will be followed by their galactic coordinates in parentheses when there is no corresponding radio source.

Column 3: Radio identification of the HII regions (Caswell & Haynes 1987) or of molecular clouds (Grabelsky et al. 1988).

Columns 4,5,6: Radial velocity with respect to the local standard of rest (LSR): Hα (mainly this paper), recombination lines (Caswell & Haynes 1987; Wilson et al. 1970), CO (mainly Grabelsky et al. 1988 and Brand et al. 1987), H_2CO (Whiteoak & Gardner 1974; Gardner & Whiteoak 1984), OH (Caswell & Robinson 1974; Manchester et al. 1970) and HI absorption lines (Goss et al. 1972).

We have grouped under the name 'Shell 290.1+0.2' several interesting filaments and patches seen in Fig. 3 and several objects which can be linked to this shell. We discuss this further in Sect. 4. Let us briefly describe known complexes not previously discussed because they lie outside the present MHS observations.

Table 2. Stellar distances

Complex	HII region	Associated star	Sp	V	B-V	U-B	β	A_v	m_o-M	d
289.3-0.6										8.0
	289.063-0.355	Wr I 18	(06)	13.88	0.96	-0.19		4.12	(14.9)	
		Wr I 19	(O9)	15.00	0.87	-0.20		3.76	(15.7)	
		Wr I 22	(O6e)	13.34	0.60	-0.51	2.508	2.99	(15.5)	
		Wr I 23	(BI)	14.36	0.68	-0.23		3.02	(14.5)	
		Wr I 25	(O6e)	13.77	0.74	-0.36		3.42	(15.5)	
		Wr I 26	(O6e)	13.42:	0.78	-0.43	2.524	3.63	(14.9)	
		Wr I 27	(B1)	14.36	0.62	-0.27		2.82	(14.7	
		Wr I 28	(B0)	13.65	0.76	-0.26		3.38	(14.2)	
		Wr I 29	(B1)	14.61	0.84	-0.10		3.53	(14.3)	
		Wr I 30	(B1)	14.32	0.73	-0.19		3.18	(14.3)	
		Wr I 35	(O6)	14.54	0.89	-0.27		3.92	(15.8)	
		Wr I 36	(O7 Iab)	12.45	1.19	-0.04	2.548	4.80	(14.2)	
	Gum 35	LS 2063	O6.5 If+WN8	10.6	0.8			3.4	(14.5)	
		Wr II 28	(O6)	13.61	0.88	-0.25		3.85	(14.8)	
		Wr II 29	(O9)	14.34	0.81	-0.26		3.58	(15.2)	
		Wr II 30	(O6)	12.89	0.80	-0.35		3.63	(14.3)	
		Wr II 31	(O7)	12.76	0.75	-0.41	2.563	3.42	(15.0)	
		Wr II 33	(O6)	14.86:	1.05	-0.14		4.43	(15.5)	
		Wr II 35	(O7 III)	11.67	0.91	-0.23	2.546	3.95	(13.4)	
		Wr II 36	(O6)	13.70	0.86	-0.27		3.79	(15.0)	
		Wr II 38	(O9)	12.58	0.44	-0.58		2.42	(14.6)	
		Wr II 39	(O9)	13.19	0.80	-0.26:		3.54	(14.1)	
		Wr II 40	(O7 Iab)	11.50	1.02	-0.15	2.538	4.25	(13.7)	
		Wr II 43	(O5 V)	12.30	0.61	-0.49	2.568	3.01	(14.7)	
	Hf 45	Wr II 42	(O5)	13.42	0.81	-0.42		3.65	(15.2)	
	Hf 46	Wr II 41	(O6)	13.25	0.83	-0.36		3.76	(14.5)	
		Sher 1	(O9/WN 4)					4.48	15.0	
		Cl 289.5-0.1	(O)					3.8	(>14.5)	
	290.487-0.814	Wr II 48	(O6)	13.76	0.85	-0.27		3.78	(15.1)	
		Wr II 52	(O6)	13.67	0.82	-0.33		3.68	(15.1)	
Shell										2.9
	Hf 44	Pis 17						1.63	13.1	
		MV 1	B0 Ve	10.46	0.20	-0.69		1.60	12.76	
		MV 2	B2 Ve	11.29	0.20	-0.62		1.41	12.35	
		MV 3	B2 Ve	11.32	0.21	-0.58		1.42	12.37	
		MV 4	B2 Ve	11.37	0.18	-0.60		1.34	12.50	
	Car OB2							1.44	12.31	
	Hα 291.2-0.2	HD 97434	O7.5 IIIn((f))	8.07	0.16	-0.79	2.58	1.47	12.22	
		LS 2225	(B0.5V)	9.57	0.12	-0.68	2.60	1.25	(12.02)	
		LS 2234	(B0V)	10.34	0.20	-0.72	2.59	1.58	(12.66)	
		HD 97581	B1 III	8.86	0.24	-0.59	2.58	1.61	11.61	
		LS 2251	B0.5 IV	9.65	0.16	-0.69	2.60	1.41	12.72	
		HD 97707	B2 Iab	8.11	0.50	-0.38	2.55	2.14	12.39	
		LS 2257	(B3 V)	11.42			2.67	1.87	(11.15)	
		NGC 3590						1.57	11.61	
		LS 2240	(B3 III)	10.37			2.61	1.61	(11.81)	
		LS 2244	(B1 V)	10.26	0.30	-0.50	2.63	1.78	11.78	
		LS 2248	(B1 V)	10.55	0.30	-0.53	2.61	1.78	11.97	
		LS 2249	(B2 V)	10.65	0.29	-0.44	2.62	(1.67)	(11.50)	
		LS 2252	(B1 V)	10.98	0.31	-0.49	2.619	1.84	(12.33)	
		N 3590 MV4	(B2 V)	11.53	0.29	-0.43		1.70	(12.3)	
290.4+1.5										2.7
	Gum 36	97471	B0 V	9.30	-0.01	-0.87		0.92	12.28	
		Br 2	(B2 V-IV)	10.60				0.87	(12.48)	
		Br 17	(B2.5)	11.38				0.94	(12.44)	
		Stock 13						0.74	12.12	

Table 2. (continued)

Complex	HII region	Associated star	Sp	V	B-V	U-B	β	A_v	m_o-M	d
290.4-2.9										4.2
	BBW 323	Br 1	(B4 V)	13.46				1.98	(12.88)	
	RCW 55	LS 2050	O6	10.71	0.47	-0.58	2.598	2.53	13.23	
		LS 2048	(B1)	11.48				2.35	(12.33)	
		LS 2044	B1 V	11.32	0.44	-0.52	2.596	2.24	12.95	
		Br 8	(B0.5V)	12.23	0.41	-0.54		2.25	(13.68)	
	BBW 331	Br 4	(B2.5V)	13.38				2.03	(13.35)	
		Br 6	(B3 V)	15.14				3.17	(13.57)	
290.6+0.2										2.8
	Gum 37	NGC 3572	O8					1.45	12.24	
		HD 97166	O7.5 IIIf	7.90	0.07	-0.89	2.579	1.22	12.30	
		HD 97222	B0.5IIn	8.79	0.19	-0.70	2.58	1.50	12.59	
		HD 97206	(B1.5V)	9.63	0.11	-0.66	2.62	1.15	(11.28)	
		HD 97207	(B1.5V)	9.55	0.12	-0.64	2.620	1.18	(11.15)	
		LS 2211	(B0 V)	10.08	0.22	-0.68	2.604	1.64	(12.31)	
		Br 4	(B1)	9.91				1.72	(11.39)	
		Br 6	(B0.5V)	9.69				1.10	(12.29)	
		Br 10	(B0.5V IV)	10.31				1.49	(12.92)	
		Br 14	(B 1.5 IV III)	11.31				1.40	(13.51)	
		Br 15	(O9 V)	9.55				1.40	(12.61)	
		Br 17	(B1 V)	10.33				1.57	(11.96)	
291.3-0.7										2.7
	Gum 38a	IR cluster								
	central part	-60°2641	B0 V	10.88	0.36	-0.72	2.579	2.11	12.65	
		HD 97499	B0.5V	9.22	0.06	-0.78	2.62	1.08	11.71	
		Br 64	(B2 V)	11.65	0.18	-0.63	2.621	1.34	(12.78)	
		Br 3	(B1 V)	9.20				1.02	(11.38)	
		Br 63	(O8.5V)	11.02				2.11	(13.47)	
	filaments	HD 97484	O8 V SB	8.39	0.31	-0.65	2.589	1.98	11.88	
		LS 2230	(B1 V)	10.67	0.26	-0.59	2.617	1.66	(12.23)	
		Br 39	(B1.5 V)	9.75				1.48	(11.07)	
	periphery	HD 97319	O7.5 III	8.52	0.22	-0.68	2.586	1.64	12.44	
		HD 97672	(O9.5V)	9.61	0.22	-0.70	2.60	1.66	(12.20)	
		Wr II 71	(B1.5V)	11.81	0.37	-0.50	2.625	1.98	(12.66)	
		LS 2265	B0 V	9.64	0.32	-0.39		1.95	11.59	
		LS 2255	(B1 Ve)	10.16	0.13	-0.73	2.46	1.22	(12.07)	
	BBW 348c	HD 98624	B1: Vne	9.81	0.27	-0.73	2.40	1.79	11.18	
		LS 2295	B2 Ve	10.55	0.08	-0.52	2.55	0.81	12.22	
		HD 98210	B0.5 III	8.79	0.05	-0.72		1.06	12.43	
		LS 2319	B1.5 III	9.68	0.06	-0.68		0.99	12.59	
		HD 98927	B1 III:nne	9.20	0.10	-0.77	2.51	1.15	12.38	
291.6-0.7										7.9
	Hf 52	Wr II 67	(O6 III)	12.55	0.94	-0.26	2.546	4.06	(14.27)	
		Wr II 63	(O6 II)	12.18	1.09	-0.12	2.538	4.58	(13.58)	
		Wr II 69	(B0 Ia)	10.30	0.93	-0.15	2.540	3.77	(13.43)	
		LS 2173	WC 6					(5.0)	(14.13)	
	Gum 38b	NGC 3603						4.48	14.49	
292.3-4.9										2.2
	RCW 58	HD 96548	WN 8	v=7.81	b-v=0.11	b-v=-0.05		1.61	11.71	
292.4+1.6										2.3
	BBW 353	Br 4	B2 V	10.48	0.11	-0.48		1.12	11.83	
294.0-1.5										2.5
	Gum 39	HD 99897	O6 V ((f))	8.35	0.16	-0.79		1.57	11.94	
	Gum 41	HD 100099	O9 III	8.07	0.10	-0.81		1.31	11.99	

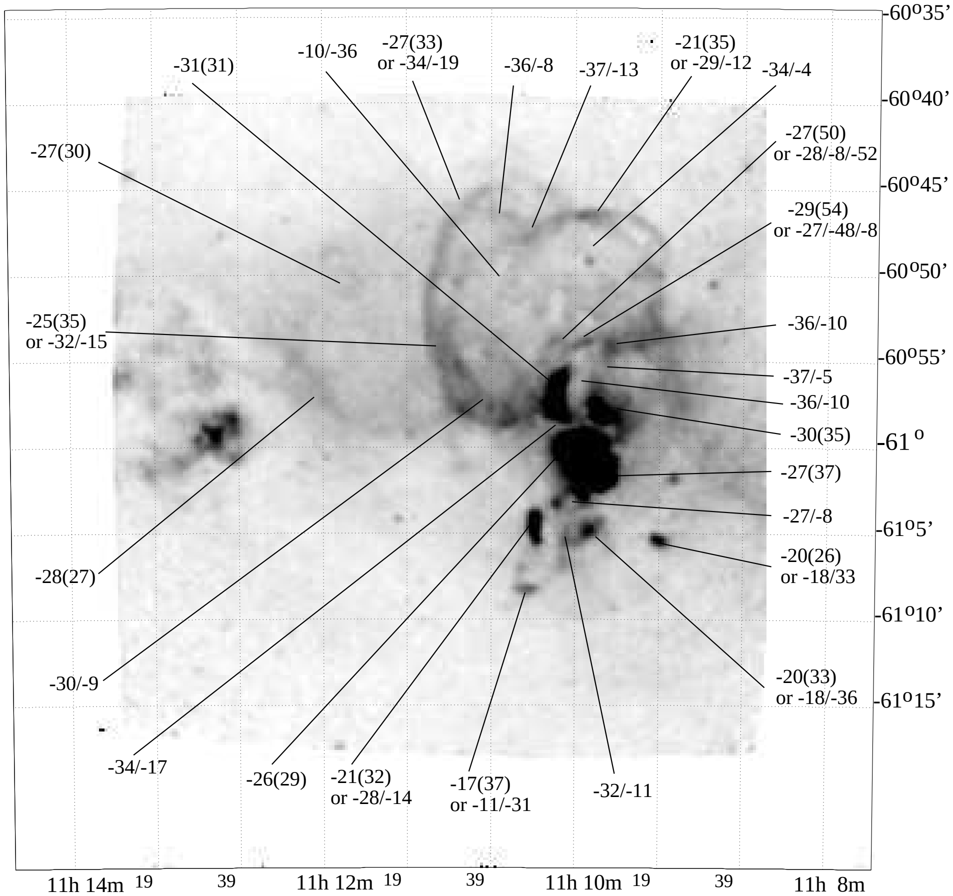

Fig. 7. Same as Fig. 4 for the HII region Gum38a (G291.3-0.7, NGC 3576).

Table 2. (continued)

Complex	HII region	Associated star	Sp	V	B-V	U-B	β	A_v	m_o-M	d
294.8-1.8										2.2
	Gum 40	HD 99898	O9 V	9.36	0.34	-0.60	2.60	2.08	11.75	
	BBW 362D	Br 30	(B2)	14.01	0.81	-0.09		3.36	(13.12)	
	BBW 362G	Br 35	B0.5V	10.20	0.08	-0.72		1.15	(12.75)	
	Gum 42	IC 2944							11.40	
		HD 101131	O6 V((f))SB	7.15	0.03	-0.89	2.576	1.15	<11.80	
		HD 101205	O7IIIn((f))SB	6.44	0.05	-0.86	2.567	1.18	<11.68	
		HD 101191	O8 V	8.50	0.04	-0.86	2.582	1.12	12.11	
		HD 101223	O8 V((f))	8.69	0.16	-0.74	2.588	1.50	11.92	
		HD 101190	O6 V((f))	7.31	0.05	-0.85	2.582	1.22	11.14	
		HD 101298	O6 V	8.07	0.07	-0.83	2.570	1.28	11.84	
		HD 101436	O6.5 V	7.59	0.06	-0.83	2.583	1.22	11.37	
295.6+0.0										1.7
	BBW 372C	Br 1	B3 V	9.97	-0.01	-0.59		0.64	10.93	
	BBW 373	Br 1	B6.5 V	11.16				0.89	(11.07)	
		Br 3	B6.5	12.29				1.10	((11.89))	

The complex 290.4+1.5 is composed of the two regions Gum36 (G290.3+1.6) and BBW 343 (G290.4+1.0). These regions are quite far from the Galactic plane but they exhibit similar CO velocity. We will see, later, that they are perhaps linked to filaments. We have grouped into the complex 290.4-2.9 small HII regions with very negative latitude and velocity ranging from -12 to -16 km s^{-1}. This range of velocity corresponds to the permitted kinematic distances of 1.8 or 4 kpc. The distance of the exciting stars are in better agreement with the far distance. Nevertheless, such velocities are also found for some patches linked to the shell 290.1+0.2. The complex 295.6+0.0 is composed of BBW 372 (G295.5+0.5) and 373 (G295.7-0.3). These regions exhibit similar velocity to 290.4+1.5 but their stellar distance rather suggests that they are at the near kinematic distance. The exciting star of BBW 357 (G294.1-2.6) has not been found by Brand (1986), so it is not possible to attribute a distance.

The complex 291.1-1.8 is a local dark cloud easily identified in Fig. 1. It is probable that the uniform diffuse ionized layer around V=0 km s^{-1} is a local layer linked to the dark cloud. Indeed, the analysis of all the other Galactic plane areas covered with the MHS, exhibit a similar diffuse component which can be attributed to the nearby Scorpio-Centaurus stellar association.

The complexes 294.0-1.5 and 294.8-1.8 are composed of the bright HII regions Gum39 (G293.6-1.3), Gum40 (G293.7-1.5), Gum41 (G294.1-2.3), Gum42 (G294.8-1.7), (= RCW60A, 60B, 61 and 62, Rodgers et al. 1960). Up to now these HII regions were grouped into the same complex assumed at the distance of IC 2944 (the exciting cluster of Gum42). This group should now be split into two subgroups with velocity between -18 and -21 km s^{-1} and -24 and -27 km s^{-1}. In this case only the HII regions of the first group would be at the distance of 2.2 kpc, while the other HII regions, which are located to the north and the east, would be linked to the complex 291.3-0.7. This last complex is located on the opposite side of the giant molecular cloud 293.3-1.4. Grabelsky (1985) suggests that this molecular cloud could be the projection of two molecular clouds with identical velocity but with different morphology. Indeed a faint link between them and an emission gap at 292.5-1.0 have been noted. From the CO maps of Grabelsky (1985) we can see 5 entities which can be linked on position and velocity arguments, to HII regions. Three entities have velocity -25 km s^{-1}. These lie between 291°2-0°5 and 292°2-2°2 linked to Gum38a, between 292°3-1°7 and 294°1-2°8 linked to Gum41, and between 292°8-1°5 and 295°0-0°1 linked to Gum39, BBW 354 (G293.4-0.9), 361 (G294.3-0.1), 363 (G294.5-0.4) and 365 (G294.5-0.3). Two have a velocity of -18 km s^{-1} which lie between 294°6-2°7 and 295°4-1°1 linked to Gum42 and between 293°5-1°4 and 294°0-1°9 linked to Gum40, BBW 362D (G293.8-1.7) and BBW 362G (G294.2-1.9).

The complex 294.0-0.9 has not been studied in Hα. It traces the far part of the Carina arm as the regions detected in Hα between 295° and 303° (Russeil 1997; Russeil et al. 1998). The complex 293.0-1.0 is an HII region with velocity of 66 km s^{-1}, placing it farther outside the Carina arm.

3.2. Distance of exciting stars

In order to identify the exciting stars of the HII regions and patches present in the mosaics we have collected from the literature all the known OB stars within a zone slightly wider than the coverage of the MHS. For each star we have collected and sorted the UBV magnitudes and the spectral type. This work was facilitated by using the SIMBAD database of the Centre de Données Stellaires de Strasbourg. This information, sorted by complex (Column 1) and by HII regions belonging to each complex (Column 2), is given in Table 2. Column 3 gives the identification of stars and clusters that may excite the HII regions along with the following notations: HD, LS (Luminous Stars, Stephenson & Sanduleak 1971), Br (Brand 1986), Wr (Wrandemark 1976) and MV (Moffat & Vogt 1975). Stars listed immediately after the cluster identification are members of this cluster. The spectral type (hereafter noted SP) is given in Column 4. When given between parenthesis it means it has been determined from photometry only. The V, B-V, U-B photometry and the Hβ equivalent width are given in columns 5 to 8. The absorption coefficient defined as Av = 3.2 [(B-V)-$(B-V)_0$], given in Column 9, has been obtained by using the intrinsic colour indices of Schmidt-Kaler (1983). Column 10 lists the distance modulus, the value between parenthesis being obtained from magnitudes without spectral type.

For clusters the distance indicated on the same line as the cluster name has been obtained by the usual main-sequence fitting method (Moffat & Vogt 1975; Lynga 1987; Shobbrook & Lynga 1994). For stars we have defined and used a SP-M_v calibration by harmonising the calibrations of Vacca et al. (1996) for the hottest stars to O9 and supergiants Iab, and Humphreys & MacElroy (1984) and Schmidt-Kaler (1983) for the dwarf and giant stars from O9.5 to B3 and spectral classes II, Ib and Ia.

The adopted distance for each complex is given in the last column on the same line as the complex identification name. Let us now discuss some particular cases.

3.2.1. The complex 289.3-0.6

The stars of this complex have been selected from their position and distance relative to the HII regions. We have noted from CO measurements that two velocity components have been detected for several regions of this complex. But, because they are based only on photometric data, the uncertainty in the stellar distance determination is large and prevents us seeing whether two groups of stars, which could be connected to the two CO components, are present. Moreover the photometric determination of Wrandemark (1976) often leads to unrealistic spectral type determination (too early) and then to an overestimated distance. Even if the mean distance is 9 kpc, we preferred to adopt the distance of LSS 2063 (8 kpc) which is, unambiguously, the exciting star of Gum35. In addition, Miller (1973) has discovered two hot star clusters, probably linked to Gum35 and 289.063-0.355, Sher 1 (289.6-0.4) and Anonymous Miller (289.5-0.1), with respective maximum distance of 5 and 8 kpc. Moffat et al. (1991) have found two hot star groups toward Sher 1. The first one has a distance of 1.9 kpc while the other, corresponding to the cluster, would be at 10 kpc.

3.2.2. The cluster Pis17

Hf 44 (=BBW 335=NGC 3503=VdBH 46, G289.5+0.1) is a very bright but small HII region excited by the cluster Pis17. The photometric distance of this cluster is 4.1 kpc (Moffat & Vogt 1975). Using the spectral types given by Herbst (1975) the mean distance would be 3.2 kpc. This last distance determination is in better agreement with the one proposed for the Shell. The velocity of Hf 44 does not allow us to distinguish it from the neighbouring filaments.

3.2.3. The cluster NGC 3603

The distance evaluation of this cluster is different from author to author: e.g. 7.0 kpc (Moffat 1983), 7.2 kpc (Melnick et al. 1989) and 5.15 kpc (Shobbrook & Lynga 1994). Crowther & Dessart (1998) have recalculated its distance from a new SP-M$_v$ calibration and recent spectrometric and photometric data of individual stars. With individual reddening obtained from observed visual colours they obtained d=7.9 kpc for E(B-V)=1.40. Using E(B-V)=1.23 obtained from combined UV and optical observation they obtained d=10.1 kpc. To be homogeneous with the other distance determinations we have adopted d=7.9 kpc which is also in ageeement with the kinematic distance.

3.2.4. Car OB2

Recently Garcia (1993) has determined UBV photometry for 470 stars and the spectral type of 105 stars in an area surrounding the Carina OB2 association, located around 11^h03^m, -59°31'. A distance of 3.1 kpc and a mean heliocentric radial velocity of V$_{hel}$=-23 km s^{-1} for the stars, and -16 km s^{-1} for the interstellar CaII were obtained. Recalculating the distance of the 40 stars of the association with known spectral type, using our SP-M$_v$ calibration and R=3.2 we find an absorption of 1.44 and a mean distance of 2.9 kpc. The southern part of Car OB2 between 290.6+0.3 and 291.3-0.3 is very rich in OB clusters at the same distance (NGC 3572, Hogg 10, Hogg 11, NGC 3590) and maybe linked together (Claria 1976; Shobbrook & Lynga 1994).

4. Discussion

4.1. The far regions

We have seen, in Sect. 2, that all positions where positive H109α have been measured have detected Hα emission. The HII regions are more widely extended than these radio positions and they are detected in Hα either as patches or as diffuse emissions. This allowed us to group HII regions into very large complexes. For example, the complexes 289.3-0.6 and 291.6-0.7 have respective diameters of about 350 pc and 180 pc.

Their kinematic distance (calculated from a flat rotation curve beyond the solar circle) is about 8 kpc, in agreement with their stellar distances (respectively 8 and 7.9 kpc). The complex 291.7-0.6 is slightly farther. Its stellar distance being unknown, we adopt its kinematic one of 9 kpc. This suggests that, at these longitudes, the Carina arm shows no extension beyond 9 kpc.

4.2. The shell

From HI data, Rizzo & Arnal (1998) have found low HI emission centred at 290.1+0.2 that they attribute to a HI shell with semi major axis 2°25' perpendicular to the Galactic plane and semi-minor axis of 1°30'. This shell has a systemic radial velocity of V$_{LSR}$=-27 km s^{-1} and an expanding velocity of 22 km s^{-1}. From the CO data of Grabelsky (1985) they find that the molecular material depicts both spatial and kinematical distribution in very good agreement with the HI. In Fig. 1 one can see that most arcs and filaments have their concavity directed towards l=290°, b=0° which is also the proposed centre for the HI shell. These filaments, visible from b=-2.2° to 3° and l=288.5° to 292.6°, are then slightly more extended than the HI shell. The longitude extension is not easy to determine because of the presence of the Carina nebula to the West and the faintness of the Hα emission to the East, which appears more as a layer than filamentary structures. In latitude, filaments could exist farther than b=3° away. Indeed, in the Survey of Parker et al. (1979) we can see high latitude ionized gas emission but it is not easy to distinguish this emission from that belonging to the extended HII region RCW 59 (G292.9+4.5). Perhaps RCW 59 is simply an extension of the filaments? This is plausible given its velocity of -22 km s^{-1} (Georgelin 1975). From the Galactic plane survey at 2.4 GHz of Duncan et al. (1995) the 3 spurs perpendicular to the galactic equator around 289.5°, 292° and 294° are probably the radio continuum counterpart of the filaments and stretched emissions visible in Fig. 1. These spurs extend to b=5°, the latitude coverage limit of their survey. Several small filaments, which they suggest is a possible SNR, are in fact entwinned in the same ensemble.

Kinematicaly the filaments of ionized hydrogen exhibit velocities between 0 and -47 km s^{-1}. The most external filaments which, assuming a radial expansion, should not have a disturbed radial velocity, fall outside the mosaics except around 292.1°, -0.5° where the measured velocity is between -23 and -24 km s^{-1} (see Fig. 3). We know also that towards BBW 353 (=VdBH 48A-E, G291.9+2.1) the CO velocity is -23 km s^{-1} (Brand 1986). The morphological and kinematical agreement of ionized hydrogen filaments and the HI Shell suggest that it is the same object that we hereafter refer to as 'the Shell'. We adopt for this Shell a systemic and expansion velocity of -23 km s^{-1} and 24 km s^{-1}. Rizzo & Arnal(1998) explain the origin of this expanding Shell by the influence of stellar winds from the most massive stars of the Car OB2 association and the cluster NGC 3572b to which we have assigned distances of 2.9 and 2.8 kpc respectively. Assuming a distance of 2.9 kpc, the dimension of the Shell is 200$\times$260 pc.

The molecular cloud 290.2-0.2 with velocity -1 km s^{-1} (Grabelsky et al. 1988) is perhaps the molecular counterpart of the moving Shell component, it corresponds to cloud G of Rizzo & Arnal (1998). The 3 other clouds they list are closed and/or belong to the giant molecular clouds GMC 288.6+1.5, V$_{LSR}$=-21.9 (cloud B), GMC 293.3-1.4 west, V$_{LSR}$=-25 (cloud C) and ETA Carina cloud, V$_{LSR}$=-19 (cloud D), Grabelsky et al. (1988). It is difficult to believe that such massive clouds have the same origin as the Shell and participate in the expansion motion. However, the velocity and distance of these GMC and associated HII regions and massive stars (as discussed in the previous section) are very close to those of the Shell. We can consider that the Shell, during its expansion, trigerred star formation in these GMCs. It would be the case of Gum38a inside GMC 293.3-1.4 west. A part of the emission surrounding Gum38a in Fig. 3, especially the 3 arcs to the west (around 11^h06^m -61°) with velocity respectively from north to south of -28, -37 and -26 km s^{-1}, would belong to the Shell. In parallel, the distance agreement of Gum37, Gum36 (G 290.3+1.6) and Hα 291.2-0.2 (at 2.7, 2.7 and 2.6 kpc) would suggest that they are also physically linked to the Shell.

Humphreys & Kerr (1974) showed that the higher HI temperature contours at 289° and 290° appear shifted to positive velocities compared with the supergiant star velocities. According to Rizzo & Arnal (1998) this neutral hydrogen anomaly can be explained by the presence of the Shell.

Using old data of Humphreys & Kerr (1974), Rizzo & Arnal (1998) interpret Gum34a,b (=RCW 54b), Gum36 (=RCW 54d) and RCW 55 (G290.3-3.0) as a bunch of HII regions that may be physically related to the HI expanding structure. We have shown that Gum34a and b are not true individual HII regions, but they are the brightest filaments of the Shell. Moreover, this is supported by the fact that the 3 supposed exciting stars (Humphreys 1972) are not hot enough to excite the regions. Gum36 has its own exciting source but exhibits significant internal motions (Georgelin et al. 1990) with a barycentric velocity varying from -20 km s^{-1} (identical to the CO velocity) to -5 km s^{-1}, towards the faint intensity zones. One can see in Fig. 1 that Gum36 (G290.3+1.6) is obviously linked to the Shell's filaments. It implies that the -5 km s^{-1} component seen on the line of sight of Gum36 could be due to the Shell. RCW 55 does not belong to the Shell. Its stellar (4.2 kpc) and kinematic (4.4 kpc) distances place it farther away.

4.3. The velocity departures

The complexes 290.6+0.2, 291.3-0.7 and the Shell exhibit an obvious velocity departure relative to the circular rotation model since their velocity is more negative by 7 km s^{-1} than any velocity permitted by the rotation model. The rotation velocity Θ of these complexes, calculated from their stellar distance and radial velocity, is 230 km s^{-1}, 10 km s^{-1} more than the solar rotation velocity or 7 km s^{-1} more than the rotation velocity Θm calculated with the galactic model of Brand & Blitz (1993) at these distances. We have looked for other velocity departures at neighbouring longitudes and distances (from the data of Russeil 1998). To the east, Gum42 does not show any departure as its velocity of -18 km s^{-1} is in agreement with its distance of 2.2 kpc. Contrarily, the Carina nebula complex (between 285° and 288°) exhibits the same deviation in Θ with a mean velocity of -20 km s^{-1} for a distance 2.6 kpc. No group nearer than 2.6 kpc exists between 285° and 293° and the farther group (beyond 4 kpc) exhibits no velocity anomaly. The velocity departure seems to concern only the complexes at distances between 2.5 and 3 kpc and between 285° and 295°; that is to say the GMC 287.5-0.5, 288.6+1.5 and 293.3-1.4 of Grabelsky et al. (1988). On the other hand, a diffuse Hα emission with mean velocity -23 km s^{-1} has been detected between 282° and 285° (Russeil 1998) more negative by about 14 km s^{-1} than the permitted velocity. The -25 km s^{-1} diffuse emission detected between 295° and 299° is in agreement with its stellar distance of 2.5 to 3 kpc. However, at these same longitudes we have found ionized hydrogen regions and diffuse emission at -40 km s^{-1} while the velocity of the tangent point is -30 km s^{-1} (Russeil 1997).

5. Conclusion

We have used one film from the AAO/UKST Hα survey (giving exceptional spatial resolution and large coverage) and a series of fields from the MHS giving velocity information, to study the Galactic plane area around longitude 290°. To clarify the spiral arm design in this area, we have attempted to delineate the large star-forming regions which are the main tracers of the arms in external spiral galaxies. This has been done by grouping the molecular clouds, HII regions and OB stars into complexes and to determine their velocity and distance.

The main conclusions are:

- In addition to the already known discrete HII regions (Gum35, 36, 37, 38a and 38b) this Galactic plane area is very rich in filaments, arcs and patches extending over several degrees, and forming an expanding Shell 4.1°×5.2° in size corresponding to the HI Shell detected by Rizzo & Arnal (1998).
- Figs. 2 and 3 give a 3-D view of the area, allowing us to distinguish the far regions (from 7.9 to 9 kpc) and the near ones (around 2.7 kpc).
- The far regions have been grouped into 3 star-forming complexes at 7.9, 8 and 9 kpc linked respectively to Gum35, Gum38b and Hf 58.
- The near regions consist of Gum37, Gum38a and the Shell.
- The HII regions Gum35, Gum37, Gum38a and Gum38b all exhibit significant internal motions.
- The velocity departures, already known around these longitudes, are of 7 km s^{-1} in Θ. They are present only through the part of the Carina arm between 285° and 295° at distances between 2.5 and 3 kpc.

Acknowledgements. D. Russeil was supported by a Lavoisier grant of the French Foreign ministry and acknowledges the hospitality of the AAO/UKST observatory, during her postdoctoral position.

References

Balick B., Boeshaar G.O., Gull T.R., 1980, ApJ 242, 584
Bok B.J., Hine A.A., Miller E.W., 1970, IAU symp.38, 246
Brand J., 1986, Ph.D. Thesis, Leiden
Brand J., Blitz L., 1993, A&A 275, 67
Brand J., Blitz L., Wouterloot J., 1986, A&AS 65, 537
Brand J., Blitz L., Wouterloot J., Kerr F.J., 1987, A&AS 68, 1
Caswell J.L., Haynes R.F., 1987, A&A 171, 261
Caswell J.L., Robinson B.J., 1974, Aust. J. Phys. 27, 597
Claria J.J., 1976, AJ 81, 155
Clayton C.A., 1986, MNRAS 219, 895
Clayton C.A., 1990, MNRAS 246, 712
Crowther P.A., Dessart L., 1998, MNRAS 296, 622
Duncan A.R., Stewart R.T., Haynes R.F., Jones K.L., 1995, MNRAS 277, 36
Garcia B., 1993, ApJS 87, 197
Gardner F.F., Whiteoak J.B., 1984, MNRAS 210, 23
Georgelin Y.M., 1975, Thesis, Universite de Provence
Georgelin Y.P., Georgelin Y.M., 1970, A&A 7, 133
Georgelin Y.M., Boulesteix J., Georgelin Y.P., et al., 1990, A&A 230, 440
Georgelin Y.M., Amram P., Georgelin Y.P., et al., 1994, A&AS 108, 513

Girardi L., Bica E., Pastoriza M.G., Winge C., 1997, ApJ 486, 847
Goss W.M., Rhadhakrishnan V., Brooks J.W., Murray J.D., 1972, ApJS 24, 123
Grabelsky D.A., Cohen R.S., Bronfman L., Thaddeus P., 1988, ApJ 331, 181
Grabelsky D.A., 1985, Ph.D. Thesis, Columbia University
Gum C.S., 1955, MNRAS 67, 155
Hartley M., Manchester R.N., Smith R.M., Tritton S.B., Goss W.M., 1986, A&AS 63, 27
Herbst W., 1975, AJ 80, 212
Hoffleit D., 1953, Harvard Ann. 119, 37
Humphreys R.M., 1972 A&A 20, 29
Humphreys R.M., Mac Elroy D.B., 1984 ApJ 284, 565
Humphreys R.M., Kerr F.J., 1974, ApJ 194, 301
le Coarer E., Amram P., Boulesteix J., et al., 1992, A&A 257, 389
Lynga G., 1987, Catalogue of Open Cluster Data. CDS Strasbourg
Manchester R.N., Robinson B.J., Goss W.M., 1970, Aust. J. Phys. 23, 751
Melnick J., Tapia M., Terlevich R., 1989, A&A 213, 89
Miller E.W., 1973, BAAS 5, 326
Moffat A.F.J., 1983, A&A 124, 273
Moffat A.F.J., Vogt N., 1975 A&AS 20, 125
Moffat A.F.J., Shara M.M., Potter M., 1991, AJ 102, 642
Noumaru J., Ogura K., 1993, PASP 105, 1269
Parker R.A., Gull T.R., Kirschner R.P., 1979, NASA SP-434
Parker Q.A., Bland-Hawthorn J., 1998, PASA 15, 33
Parker Q.A., Malin D.F., 1999, PASA 16, 228
Parker Q.A., Phillipps A., Morgan D.H., 1999, ASP Conf. Ser. 168, 126
Phelps R.L., Janes K.A., 1991, PASP 103, 491
Persi P., Roth M., Tapia M., Ferrari-Toniolo M., Marenzi A.R., 1994, A&A 282, 474
Rizzo J.R., Arnal E.M., 1998, A&A 332, 1025
Rodgers A.W., Campbell C.T., Whiteoak J.B., 1960, MNRAS 121, 103
Roger R.S., Milne D.K., Caswell J.L., Little A.G., 1986, MNRAS 219, 815
Russeil D., 1997, A&A 319, 788
Russeil D., 1998, Thesis, Universite de Provence
Russeil D., Georgelin Y.M., Amram P., et al., 1998 A&AS 130, 119
Russeil D., Castets A., 2000, A&A submitted
Russeil D., Parker Q., 2000, submitted
Shobbrook R.R., Lynga G., 1994, MNRAS 269, 857
Stephenson C.B., Sanduleak N., 1971, Publ. Warner Swasey Obs. 1 n 1
Schmidt Kaler Th., 1983, Landolt-Borstein, New Series, Group VI Vol. 2B, 14
Vacca W.D., Garmany C.D., Shull J.M., 1996, ApJ 460, 914
van den Bergh S., Herbst W., 1975, AJ 80, 208
Whiteoak J.B., Gardner F.F., 1974, A&A 37, 389
Wilson T.L., Metzger P.G., Gardner F.F., Milne D.K., 1970 A&A 6, 364
Wrandemark S., 1976, A&AS 23, 231